Supporting Information:

Plasmon-driven motion of an individual molecule

Tzu-Chao Hung, Brian Kiraly, Julian H. Strik, Alexander A. Khajetoorians, and

*Daniel Wegner**

Institute for Molecules and Materials, Radboud University, Nijmegen, The Netherlands

*Correspondence to: daniel.wegner@ru.nl

The supporting information includes:

S1 Experimental details

We performed the STM and STM-LE measurements using an Omicron ultra-high vacuum low-temperature STM system operated at $T = 4.5$ K with a base pressure below $1 \cdot 10^{-10}$ mbar.[1] All experiments shown here were performed for ZnPc molecules adsorbed on 3 ML NaCl/Ag(111) (for additional data on 2 ML NaCl/Ag(111), see section S4). All STM-LE spectra presented in the main text were acquired using the same plasmonic tip (cf. Fig. S1), and measured on the same ZnPc molecule, in order to eliminate tip-dependent variations in the STM-LE spectra. All relative changes reported for a given STM-LE spectrum were reproducible with different microtips (see, e.g., section S4).

An adapted photon collection apparatus was used in our experiment.[2] An *in-situ* lens (diameter = 10.0 mm, focal length = 15.0 mm, VIS-NIR coated, plano-convex, Edmund Optics Ltd.) was placed ca. 15 mm away from the tunnel junction with an angle of 25° to the surface to collimate the photons and subsequently guide them through the cryoshield and UHV viewports. An *ex-situ* lens (diameter = 25.0 mm, focal length = 50.0 mm, uncoated, Thorlabs) redirected the light into an optical fiber bundle which was connected to a grid spectrometer (SpectraPro HRS-300, Princeton Instruments) equipped with a LN_2-cooled CCD detector (PyLoN 100, Princeton Instruments). The entrance slit to the spectrometer was set to a width of 200 μm for all the reported spectra. Three different gratings were used in our experiment. The low spectral resolution grating (150 grooves/mm, 12.4 meV) was used to characterize the plasmon resonance of the tip. The mid (600 grooves/mm, 2.9 meV) and high (1200 grooves/mm, 1.3 meV) spectral resolution gratings were used when characterizing the main transition peak of the molecules.

For the sample preparation, a Ag(111) single crystal (MaTeck) was cleaned by multiple cycles of sputtering and annealing, followed by deposition of NaCl from a Knudsen cell while the Ag(111) surface was kept at room temperature. The sample was then transferred into the

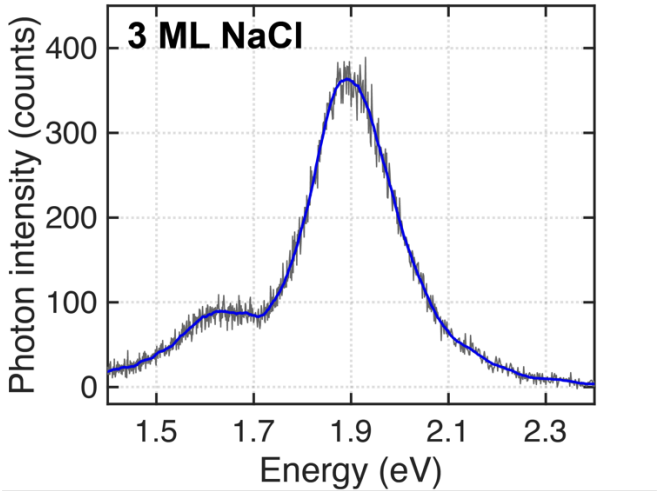

Figure S1. Plasmon resonance spectrum of the tip used for the presented STM-LE data. A broad plasmon resonance band, acquired on 3 ML NaCl/Ag(111), was intentionally tuned around 1.9 eV (V_S = –2.5 V, I = 100 pA, t = 60 s). Raw data is plotted as gray solid line, the blue solid line is a 60-point Savitzky-Golay filtered curve of the raw data.

cryogenic STM and cooled to base temperature. ZnPc molecules (97%, Sigma-Aldrich) were thermally evaporated from a Knudsen cell and deposited onto the cold NaCl/Ag(111) sample (T < 6 K) inside the STM. STM images were taken both in constant-current and constant-height mode (as stated), with dI/dV_S spectra and maps obtained using a lock-in technique with a modulation voltage V_{rms} = 5 mV at a frequency of 819 Hz and 437.1 Hz, respectively.

To enhance the optical STM-LE output, we created Ag-coated W tips by controllably indenting flashed W tips into the Ag(111) crystal,[3] followed by further modification through dipping and voltage pulsing on bare Ag to achieve the desired plasmon resonance (i.e. around 1.9 eV, close to the energy of the Q(0,0) transition). The photon collection efficiency was determined to be sufficient when the maximum intensity of the plasmon resonance spectrum acquired on 3 ML NaCl/Ag(111) reached more than 100 counts using feedback parameters of V_S = –2.5 V, I = 100 pA and an acquisition time of t = 60 s). Fig. S1 shows a typical plasmon resonance spectrum after such optimization. This particular spectrum corresponds to that of the

tip used for all STM-LE spectra shown in the main text. We note that the measurements presented in section S6 were performed with a bulk Ag tip.

S2 Molecular orbitals of isolated ZnPc and anchored ZnPc

The HOMO and degenerate LUMO/LUMO+1 have 4-fold symmetry in the free-standing ZnPc molecule.[4,5] Experimentally, the local density of states (LDOS) of molecular orbitals (MOs) can be observed using dI/dV_S mapping. Fig. S2 shows the constant-height dI/dV_S maps of the HOMO and LUMO of the isolated and anchored ZnPc molecules. The HOMO of the isolated ZnPc is shown in Fig. S2(a), with the expected four-fold symmetry. Alternatively, on ultrathin NaCl one can also visualize the MOs using constant-current or constant-height STM images,

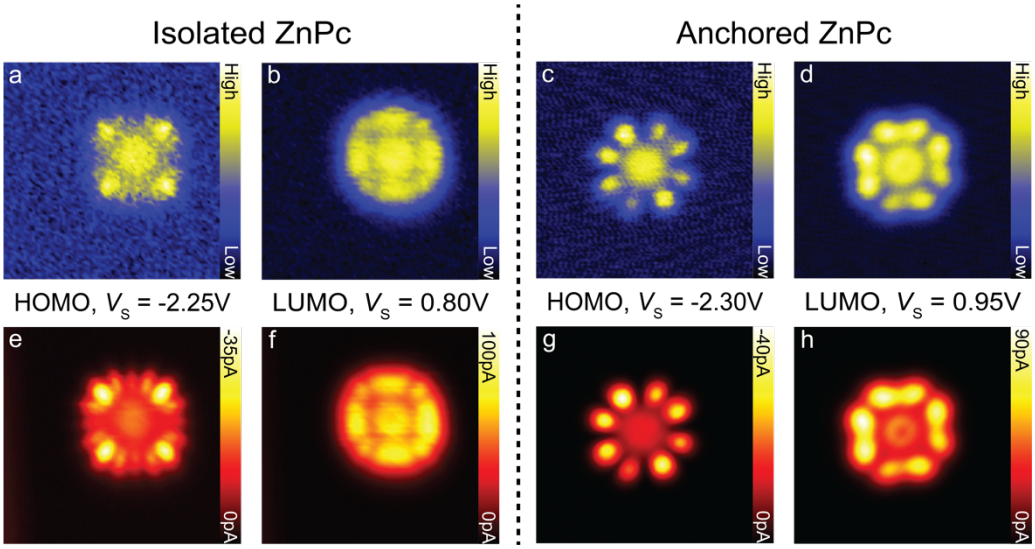

Figure S2. Molecular orbitals of isolated ZnPc and anchored ZnPc. (a-d) The constant-height differential conductance maps (4×4 nm^2) show (a) the HOMO of the isolated ZnPc (V_S = –2.25 V), (b) the LUMO of the isolated ZnPc (V_S = 0.80 V), (c) the HOMO of the anchored ZnPc (V_S = –2.30 V), and (d) the LUMO of the anchored ZnPc (V_S = 0.95 V). (e-h) Simultaneously acquired constant-height STM images corresponding to (a-d). The feedback loop was opened at the center of the molecule at V_S = –2.5 V and I = 100 pA for the isolated molecule and V_S = –2.5 V and I = 50 pA for the anchored molecule.

as there is negligible LDOS within the HOMO-LUMO gap when molecules are adsorbed on insulators.[6]

In Fig. S2(e), the constant-height STM image provides better resolution of the MOs. The observation of 16 distinct lobes (same feature in Fig. 1(b)) in this current map confirms the ±11° shuttling motion of the molecule with respect to the NaCl film.[7] The degenerate LUMO/LUMO+1 reveals the expected 4-fold symmetry in Fig. S2(b) and Fig. S2(f). To ensure the symmetry of the MOs remained the same upon anchoring the molecule to the NaCl step edge, the same measurements were performed on the anchored molecules. Fig. S2(c) shows the HOMO of the anchored molecule, where eight lobes are observed (compared to the 16 from Fig. S2(a)) because the molecule was no longer shuttling (see also Fig. 1(c)). Fig. S2(d) shows the 4-fold symmetry of the LUMO/LUMO+1, which indicates that the presence of the NaCl step edge did not break the degeneracy of these orbitals. The maps in Fig. S2(c, d, g, h) are consistent with the STS data (Fig. 1(d)), which shows that the electronic state of the molecule was not modified when the molecule was anchored to the NaCl step edge.

S3 STM-LE response of ZnPc due to the presence of defects and the NaCl Moiré pattern

We found that the optical response of single ZnPc molecules is very sensitive to the surrounding environment. Here, we give two illustrative examples: (1) defects in the vicinity of the anchored the molecule, and (2) the molecule pinned to a point defect.

Fig. S3(a) shows a STM constant-current image obtained at negative bias (V_S = –2.3 V), with a ZnPc molecule anchored to a step edge. However, when imaging at positive bias (V_S = 2.3 V), several defects could be observed in the vicinity of the molecule (Fig. S3(b)). To understand the electronic properties of the molecule, under the influence of these defects, the molecular orbitals (MOs) were mapped using constant-height dI/dV_S maps. The HOMO of the

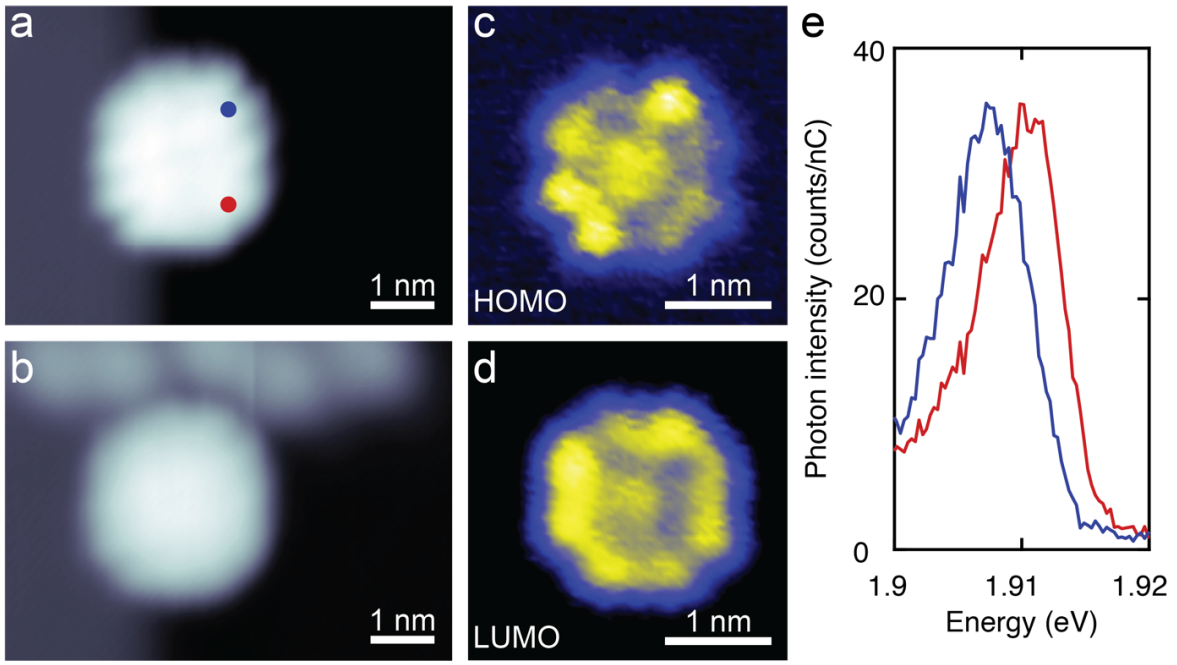

Figure S3. Degeneracy breaking by defects in the vicinity of an anchored molecule. (a) Constant-current STM image taken at V_S = –2.3 V shows no defect present (I = 15 pA). (b) Constant-current STM image taken at V_S = 2.3 V uncovers defects in the NaCl next to the molecule (I = 15 pA). (c) Constant-height dI/dV_S map of the HOMO and (d) the LUMO of the anchored molecule, revealing a two-fold symmetry of the latter. The feedback loop was opened at the center of the molecule at V_S = –2.5 V and I = 100pA. (e) STM-LE spectra acquired at the positions marked in (a) show a shift of the fluorescence (V_S = –2.5 V, I = 100 pA, t = 180 s).

anchored ZnPc shows 4-fold symmetry in the dI/dV_S map (Fig. S3(c)). However, in Fig. S3(d), the symmetry of the LUMO/LUMO+1 is reduced from 4-fold to 2-fold, which implies that the degeneracy of the LUMO and LUMO+1 was broken due to the presence of the defect. Furthermore, STM-LE spectra taken at two neighboring phenyl arms of the Pc ligand (tip positions are shown in Fig. S3(a)) reveal that the Q(0,0) transition peak is located at different energies, implying that the two orthogonal transition dipoles of the ZnPc were no longer degenerate, consistent with the 2-fold symmetry seen in the dI/dV_S map. This example demonstrates that even remote defects (i.e. without direct physical contact) can have an

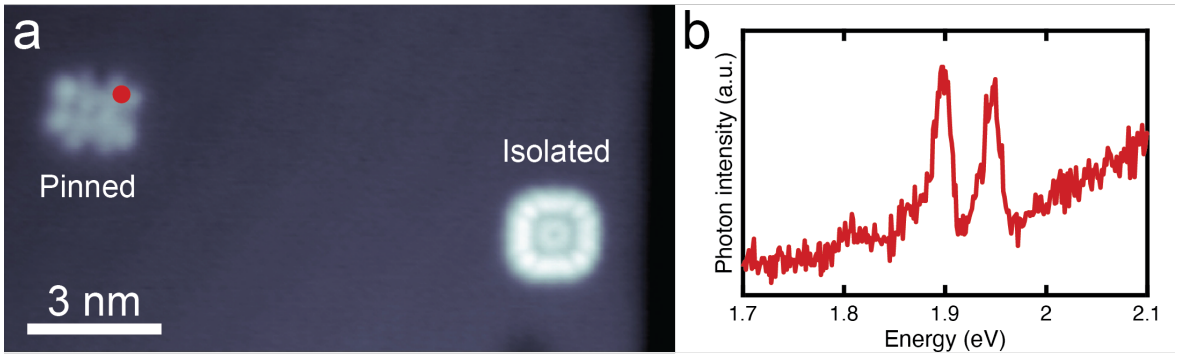

Figure S4. Defect-pinned ZnPc. (a) A ZnPc was intentionally manipulated on top of a NaCl surface defect, the constant-current STM image shows the defect-pinned ZnPc and an isolated ZnPc (V_S = 0.8 V, I = 15 pA). (b) STM-LE spectrum acquired on the defect-pinned ZnPc (position marked in (a)) revealing a strongly modified fluorescence response (V_S = -2.5 V, I = 200 pA, t = 300 s).

influence on the properties of the ZnPc. We speculate that the defects here are most likely Cl vacancy sites.[8] The breaking of degeneracy of the LUMO/LUMO+1 and the transition dipoles of the ZnPc could be attributed to local electric fields, as the vacancies lead to a local charge accumulation.

The effect of a point defect in the NaCl surface in direct contact with the ZnPc is summarized in Fig. S4. Here, a ZnPc molecule was pinned on top of a defect (presumably also a Cl vacancy) using STM manipulation. The defect-pinned ZnPc showed a severe distortion in the STM constant-current image (Fig. S4(a)), indicating that the electronic properties were strongly influenced by the underlying defect. Moreover, this pinned ZnPc exhibited unusual optical properties (Fig. S4(b)): multiple peaks were observed in the STM-LE spectrum. The spectra were also strongly site-dependent (not shown).

To avoid these complicating issues, we ensured that NaCl step edges were atomically pristine prior to anchoring a ZnPc to it. For the results shown in the main text; the step edges were checked by using constant-current imaging at both polarities. A region was considered clean when no defect was found within a radius of 3 nm around the position where a ZnPc

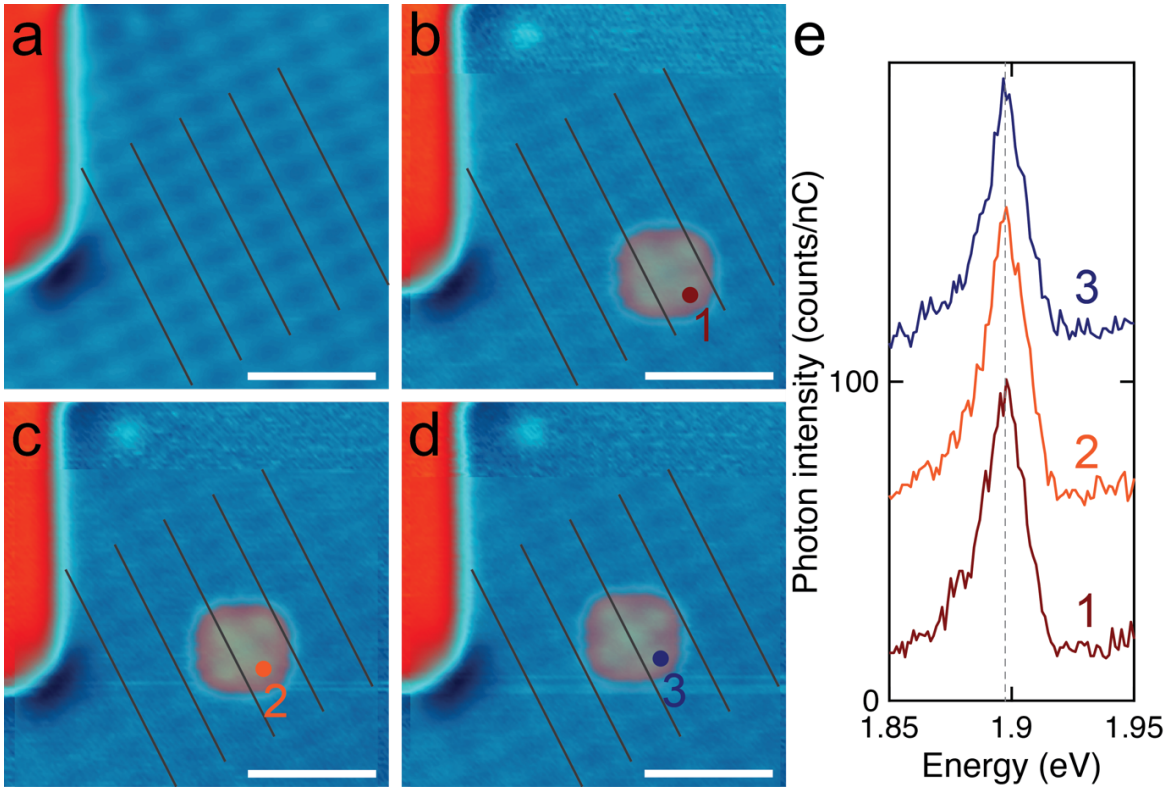

Figure S5. ZnPc on different adsorption sites of the Moiré pattern. (a) Constant-current STM image of 2 ML NaCl/Ag(111), resolving the structural Moiré pattern of the NaCl layer (cf. gray lines to guide the eye) (V_S = 2.5 V, I = 20 pA, scale bars = 3 nm). (b-d) A single ZnPc molecule was manipulated onto the area shown in (a) and placed on different locations within the Moiré pattern. The images are overlaid onto that shown in (a) with 60% transparency (V_S = –2.5 V, I = 6.5 pA). (e) STM-LE spectra of the ZnPc at different adsorption sites, as labelled in (b-d) (V_S = –2.5 V, I = 100 pA, t = 30 s).

would later be anchored. We note that we also carefully checked the potential impact of the NaCl Moiré pattern on Ag(111) (Fig. S5) on the STM-LE spectra of ZnPc,[9] but we essentially found no influence, i.e. STM-LE spectra of isolated ZnPc were always identical (Fig. S5(e)), irrespective of the location of the molecule within the Moiré pattern.

S4 Lamb shift modulation of anchored ZnPc on 2 ML NaCl

An orientation-dependent measurement (comparable to Fig. 2) was also done on an anchored ZnPc molecule on 2 ML NaCl/Ag(111) (i.e., anchored to a 3 ML step edge), using a different

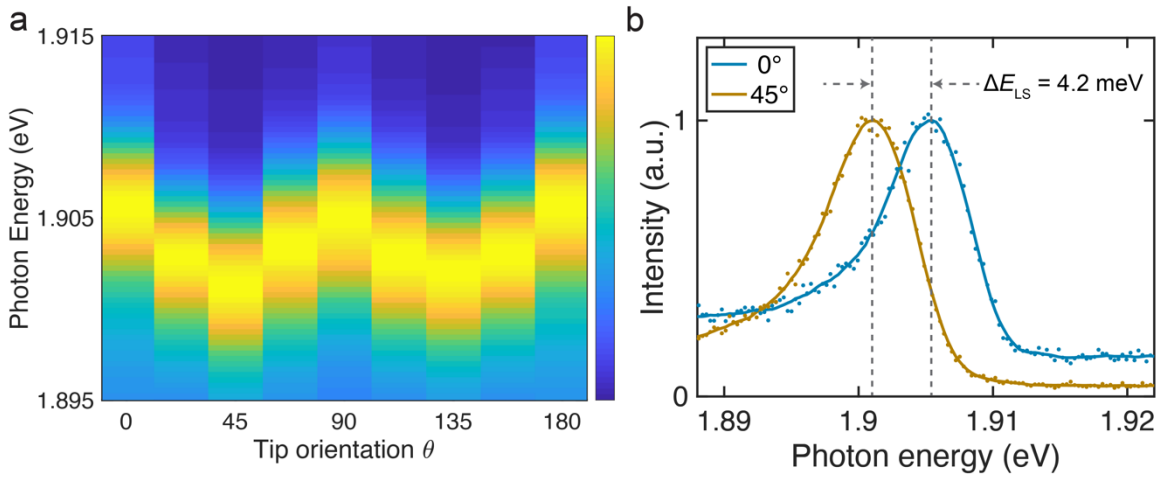

Figure S6. Lamb shift modulation of anchored ZnPc on 2ML NaCl/Ag(111). (a) Color plot of normalized STM-LE spectra showing periodic modulation of the Lamb shift. (b) Two typical Fano-peak STM-LE spectra taken on top of anchored ZnPc (r = 0.92 nm) for θ = 0° and θ = 45° (cf. Fig. 1(c)), with ΔE_{LS} = 4.2 ± 0.3 meV (taken in constant-current mode, V_S = –2.5 V and I = 100 pA, t = 180 s). The solid lines are 20-point Savitzky-Golay filtered curves of the raw data.

plasmonic tip. Fig. S6(a) summarizes the STM-LE spectra of the Q(0,0) transition peak as a function of θ from 0° to 180°, where r = 0.92 nm. The resulting series of STM-LE spectra reveals that the emission peak position oscillates with a π/2 periodicity. The equal energy level shift at 45° and 135° can be attributed to the tip shape (plasmonic nanocavity) being close to point-symmetric. To analyze this further, we plot STM-LE spectra at θ = 0° (blue) and at θ = 45° (orange) (Fig. S6(b)). The Lamb shift is largest at θ = 45°, which is redshifted relative to the spectrum at θ = 0°. The spectral Fano profiles and widths are comparable. A fit of the spectra with a Fano function yields a LSM of ΔE_{LS} = 4.2 ± 0.3 meV for the anchored ZnPc on 2 ML NaCl/Ag(111). When compared with the results on 3 ML NaCl (Fig. 2), it is clear that the absolute energies of the Q(0,0) transition depend on the thickness of the decoupling layer, but the LSM does not.

S5 Fitting STM-LE spectra by Fano profiles

In general, a Fano profile reflects the coherent coupling between a discrete state and a continuum of states. The interplay between the inelastically tunneling electrons, the exciton of the molecule, and the plasmonic resonance has previously been suggested to fulfill these criteria.[10,11] Here, we fit our STM-LE spectra using the equation $F(E) = A \cdot f(E) + B$, where A is a scaling factor, B accounts for an offset background intensity, E is the photon energy, and f is the Fano function[12]

$$f(q, \Gamma, E_0; E) = \frac{\left(q + \frac{E - E_0}{\Gamma}\right)^2}{1 + \left(\frac{E - E_0}{\Gamma}\right)^2}$$

with the Fano asymmetry parameter q, the resonant energy of the exciton E_0, and the linewidth (half width at half maximum) of the resonance Γ. The asymmetry parameter, q, roughly reflects the ratio of the different excitation channels responsible for forming the molecular exciton. Plasmon-induced exciton formation dominates for $|q| < 1$, leading to an asymmetric dip feature in the resulting STM-LE spectrum, as seen in the spectra taken near an isolated molecule

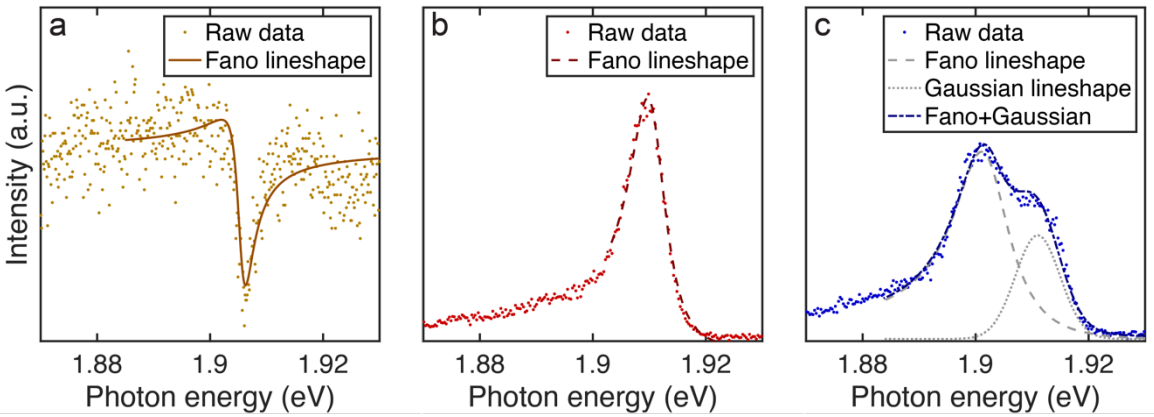

Figure S7. Fano lineshape fitting. STM-LE spectra taken at (a) close proximity to an isolated ZnPc (b) an anchored molecule, and (c) isolated ZnPc. Raw data are plotted as dots and the solid lines are the fitting results with asymmetry parameter $q = -0.47 \pm 0.08$, -4.9 ± 0.3, and -6.7 ± 1.8 respectively.

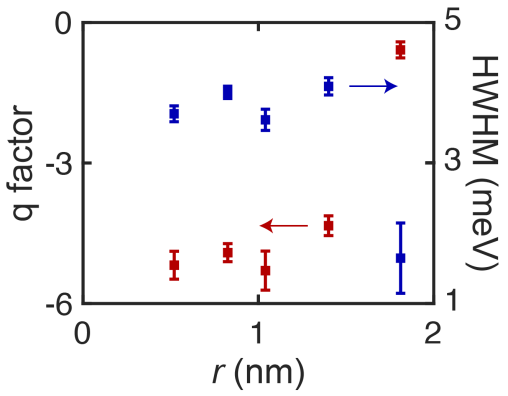

Figure S8. Radius-dependent Fano fitting parameters. Radius dependence of the fitted Fano asymmetry parameter q (red squares) and the fitted half width half maximum Γ (blue squares). The azimuthal angle was fixed at 45° (along the phenyl arm). STM-LE spectra at r = 0.52 nm were taken in constant-height mode with feedback loop opened at the ZnPc center (V_S = –2.5 V, I = 150 pA, t = 120 s). STM-LE spectra at r = 0.83 nm and 1.04 nm were taken in constant-height mode with feedback loop opened at the ZnPc center, V_S = –2.5 V, I = 500 pA, t = 120 s. STM-LE spectra at r = 1.40 nm and 1.81 nm were taken in constant-current mode (V_S = –2.5 V, I = 200 pA, t = 60 s).

(Fig. S7(a)). On the other hand, dominant exciton formation from electrons resonantly tunnel into/out of the molecule is reflected by $|q| > 1$, resulting in an asymmetric peak in the STM-LE spectrum. This is seen in the spectra taken on top of an anchored molecule (Fig. S7(b)). We did not observe a significant radius-dependent variation of q when the tip was still located on top of the phenyl arm ($\theta = 45°$, Fig. S8) but a sudden jump to $|q| < 1$ for r > 1.5 nm. As all cases are nicely fitted by the Fano function, we conclude that the discrete exciton state coupled to the continuum of the plasmonic cavity fulfill the Fano criterion.

We note that a simple Fano profile is not sufficient to reproduce the spectrum taken on top of the isolated ZnPc due to the shoulder at higher energy. An additional peak was needed to fit the spectrum of the isolated ZnPc. Surprisingly, we were not able to adequately fit the shoulder with a second Fano profile, rather the best fit was made by a Gaussian peak (Fig. S7(c)). Although the underlying reason for the Gaussian lineshape is unclear, the fit enables the

extraction of reliable values for the main transition peak (1.902 eV) and a good estimation for the position of the shoulder (1.911 eV). We note that the fit results of the main peak do not change significantly when fitting the shoulder with a Fano or a Lorentzian profile.

S6 Verification of remote shuttling and quantification of the switching behavior

In order to verify that the ZnPc molecules indeed shuttle between the +11° and –11° orientations during the remote STM-LE measurements, we utilized the fact that in a wide voltage range within the HOMO-LUMO gap (cf. Fig. S10 and discussion below) the molecules do not shuttle

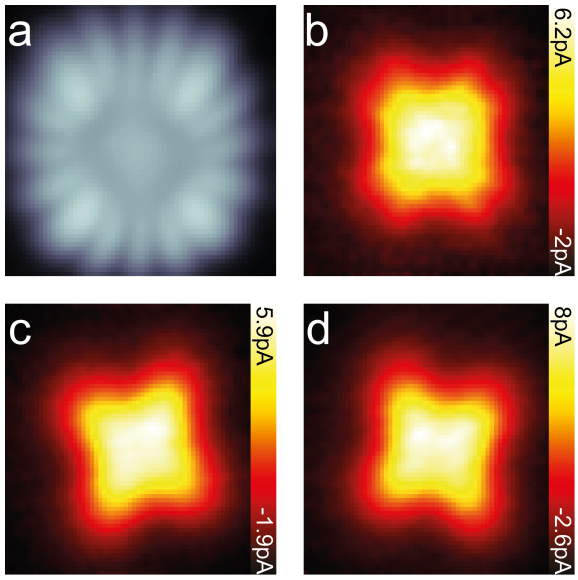

Figure S9. In-gap imaging the bistable orientations. (a) Constant-current STM image of an isolated ZnPc molecule on 3 ML NaCl/Ag(111) measured at V_S = –2.5 V, I = 10 pA, revealing rapid shuttling. (b) In-gap constant-height STM image of the same molecule at V_S = 0.4 V. The molecule still shows rapid shuttling, leading to a superposition of the ±11° in-gap shape of the molecule. (c) In-gap constant-height STM image of the same molecule at V_S = 0.2 V. At this voltage, no shuttling is observed, and the molecule can be imaged in the +11° orientation. (d) Same as (c), after shortly inducing shuttling at higher voltage. Now the molecule is oriented in the –11° orientation. For the constant-height imaging in (b-d), the feedback loop was opened at the center of the ZnPc at V_S = –2.5 V, I = 200 pA. All images are 2.5 × 2.5 nm^2.

and can be imaged in either of the bistable orientations. This is demonstrated in Fig. S9 for an isolated ZnPc on 3 ML NaCl/Ag(111). Resonant tunneling into the HOMO induces rapid shuttling, and the STM image appears as a superposition of the ±11° oriented HOMO spatial distributions (Fig. S9(a)). Within the gap (b-d), the molecule appears as a blurred cross-like feature. Above the threshold voltage for rapid shuttling (Fig. S9(b)), this feature is still symmetric about the NaCl crystallographic axes. However, below the threshold (Fig. S9(c,d)) molecules do not shuttle anymore but are fixed in one orientation. As a consequence, the cross-like feature is clearly rotated by about 11°, and both +11° (Fig. S9(c)) and –11° (Fig. S9(d)) orientations can be observed.

The threshold voltages at which remote shuttling starts to occur, and a rough measure of the probability to find a molecule in the other orientation after a pulse can be determined by repeated application of voltage pulses at a certain distance away from the molecule using a particular polarity and magnitude, and subsequent in-gap imaging of the molecular orientation. This is demonstrated in Fig. S10(a), where two molecules are first imaged at 0.2 V to determine their orientations. Then the tip is moved laterally to a position ca. 2.3 nm away from the center of both molecules, and a voltage pulse is applied for ca. 5 seconds at the same constant-height condition at which the image was taken. Afterward the voltage is changed back to 0.2 V and the molecules are imaged again to check if their orientation has changed. In the example of Fig. S10(a), one of the molecules has changed its orientation. For each voltage, we repeated this sequence several times to acquire statistics of the probability to find a molecule in a different orientation. This is summarized in Fig. S10(b). As can be seen, no switching occurs in a range between –1.3 V and +0.4 V. We note that we cannot rule out that a molecule switched more than once during a voltage pulse. In fact, for larger biases we expect rapid shuttling to occur. In that scenario, the maximum probability to find a molecule in the other orientation after the pulse is 50%. Indeed, for voltages below –2 V, this plateau is reached. However, as it is not

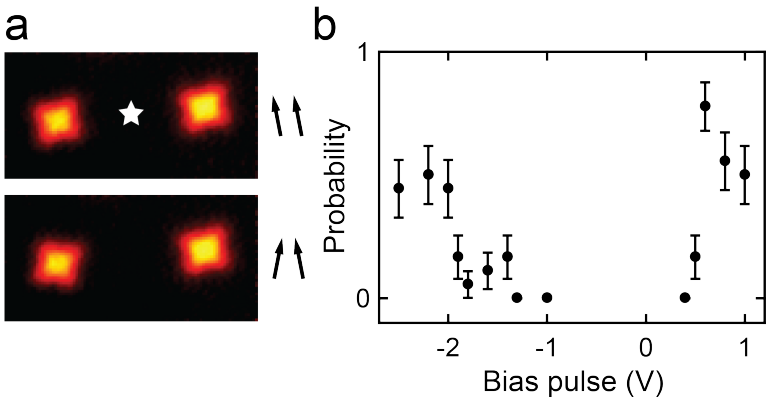

Figure S10. Voltage dependence of remote activation of the ZnPc shuttling motion. (a) Two constant-height STM images taken at V_S = 0.2 V before (top) and after (bottom) moving the STM tip to the position marked by a star and applying a voltage pulse of –2.5 V at constant height for ca. 5 seconds. The left-hand molecule switched its orientation, while the right-hand molecule shows the same orientation. (b) Statistics of probability to find a molecule in a different orientation after application of a 5-second bias pulse with different voltage at the position marked in (a). For each voltage, this experiment was performed 9 times, leading to a total of up 18 observable switches. Error bars correspond to binomial distribution standard deviations. All experiments were performed at constant height, which was defined by opening the feedback loop at the ZnPc center at V_S = –2.5 V, I = 200 pA. The images are 8 × 4 nm^2

possible to monitor the motion of the molecule in time while the STM tip is parked several nanometers away, a quantitative analysis of the remote switching statistics is limited. Moreover, the probabilities depend on the chosen vertical tip-sample distance as well as the lateral distance of the pulse position relative to the molecule (in both cases decreasing with increasing distance), and they vary with different tips. Qualitatively, however, the results of Fig. S10(b) are reproducible.

The provided data allows us to rule out possible mechanisms that may activate the shuttling motion. One possible scenario may be energy transfer from ballistic transport of hot electrons. Studies have shown that on conductive surfaces, remote injection of tunnel currents and ballistic transport through the substrate can remotely modify molecules adsorbed on the surface.[13-17]

However, in our case, the NaCl insulating film prevents hybridization of the ZnPc with metallic substrate states. Therefore, hot electrons would have to tunnel through the NaCl layers in order to transfer energy into the molecule. Apart from the fact that this process seems not very likely, it could only occur at energies corresponding to the HOMO (LUMO) at negative (positive) bias. As we already observe shuttling at voltages that are lower in magnitude than the onset energies of the HOMO (–2.15 eV) and the LUMO (+0.85 eV), as deduced from STS spectra (cf. Fig. 1(d)), we can rule out hot electrons in the metal substrate as a mechanism that activates remote shuttling.

Plasmon-exciton coupling is a second possibility of remote energy transfer, as the nanocavity plasmons have a spatial extent of a few nanometers. In this scenario, a plasmon excites the ZnPc into the S_1 excited singlet state. Through vibronic coupling, the molecule can relax to a higher-lying vibrational state of the electronic S_0 ground state. This vibrational energy could suffice to overcome the energy barrier between the bistable adsorption sites,[18-20] hence inducing the shuttling. However, the required energy to excite the molecule to the S_1 state is about 1.9 eV, and the maximum energy of the nanocavity plasmons is determined by the applied tunneling voltage. Hence, we can rule out plasmon-exciton coupling as the origin for shuttling motion for all $|V_S| < 1.9$ V. At larger voltage magnitudes, plasmon-exciton coupling may offer an additional activation channel for rapid shuttling.

Switching of ZnPc between the two adsorption orientations could also be due to a field effect caused by the strong electric fields between tip and sample, which can in principle induce adsorbate motion several nm away from the tip apex.[21-23] Usually, electric field-based switching events are independent of the bias polarity. In the present case, the observed threshold bias for shuttling is very different for positive *vs.* negative bias by more than a factor of 3. This suggests that an electric field effect can be ruled out as the mechanism for the ZnPc shuttling motion.

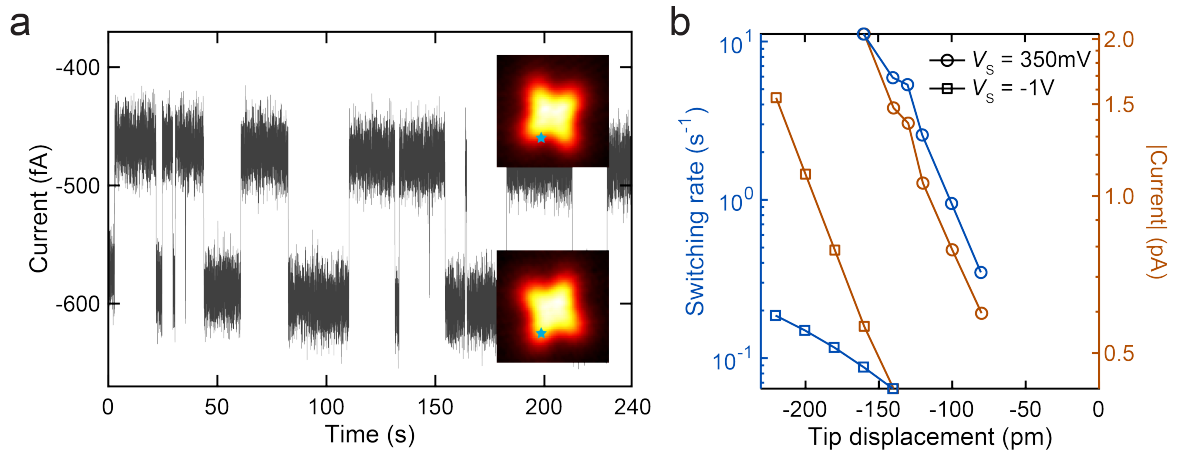

Figure S11. Vertical distance-dependent dynamics of the ZnPc shuttling motion. (a) Telegraph noise of the ZnPc shuttling between the +11° (bottom) and –11° (top) orientation. The tip is laterally positioned such that it is on top of a ZnPc lobe in the +11° orientation (see marked position in both inset STM images), and the time-dependent evolvement of the tunnel current is measured with the feedback loop opened at the center of the ZnPc at V_S = –2.5 V, I = 10 pA. (b) Switching rate (blue) and tunnel current (orange) as a function of vertical tip displacement for two different in-gap sample biases, revealing an exponential increase of both with decreasing tip-sample distance.

We can gain more detailed understanding of the shuttling mechanism by investigating the dynamics directly in time. For this purpose, we park the STM tip directly above one of the lobes of the ZnPc molecule when it is in the +11° orientation (see inset STM image in Fig. S11(a)), and we measure the tunnel current *vs.* time at constant tip-sample distance. We repeat the measurement for various tip-sample distances. Here, a zero tip displacement is defined by the tip-sample distance at which the tip was parked above the center of ZnPc at V_S = –2.5 V, I = 10 pA, and smaller (i.e. negative) displacements refer to a decrease of the tip-sample distance. The time trace of the tunnel current (Fig. S11(a)) reveals telegraph noise, with larger current magnitude whenever the molecule is in the +11° orientation (i.e., the lobe is located underneath the tip) and a smaller magnitude when the ZnPc has switched to the –11° orientation. A statistical analysis of the telegraph noise, as previously used by Kiraly *et al.*,[1] allows us to

extract the switching rate as a function of tip-sample distance for a given sample bias. We note that the voltage range at which we can perform such experiments is limited by the bandwidth of the current preamplifier. We used in-gap voltages far below the onset values of the HOMO and LUMO, respectively in order to rule out direct resonant tunneling into a molecular orbital, which could also induce rapid shuttling.[24,25] We further note that quantitative values depend on the tip, which is why we used the same tip in all measurements presented in Fig. S11.

Fig. S11(b) summarizes the switching rates (blue) as well as the tunnel currents (orange) as a function of vertical tip displacement for two different in-gap sample biases. Compared to measurements done at $V_S = -1$ V the switching rate at $V_S = 350$ mV is more than two orders of magnitude larger, despite its smaller magnitude, and changes much faster with the vertical tip displacement. At both voltages, the switching rate increases exponentially with decreasing tip-sample distance. These findings provide additional evidence that the shuttling cannot be caused by an electric field effect, where an inverse distance dependence as well as a polarity-independent behavior would be expected. As expected from a tunnel junction, also the tunnel current increases exponentially with decreasing tip-sample distance. As the used in-gap voltages rule out direct tunneling into molecular orbitals, this current refers to tunneling between the tip and the metal substrate.

The data can be understood when considering plasmon-molecule coupling as the energy transfer mechanism to induce shuttling motion. The strength of the plasmon resonance is directly proportional to the tunnel current, as the excitation of plasmons occurs via inelastic tunneling of electrons between the tip and the metal substrate.[26-28] Therefore, if plasmon-molecule coupling causes the shuttling, we would also expect an exponential distance dependence of the switching rate. Moreover, the significantly different behavior at positive *vs.* negative bias can be understood by the nanocavity plasmons. We reproducibly find that the intensity of the plasmon resonance in STM-LE spectra is more than one order of magnitude

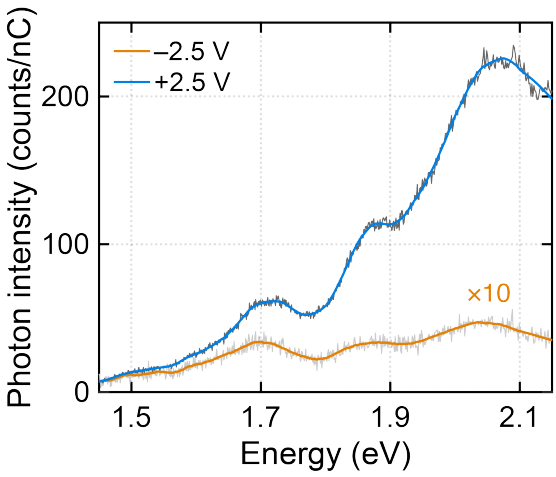

Figure S12. Polarity dependence of the plasmon resonance. STM-LE spectra on 3 ML NaCl/Ag(111) using the bulk Ag tip applied in the switching experiments at V_S = –2.5 V and +2.5V (I = 200 pA, t = 120 s and 60 s). We reproducibly observe for both Ag-coated W tips as well as Ag bulk tips that the plasmon resonance is more than an order of magnitude more intense at positive polarity. Raw data is plotted as gray solid line, the blue and orange solid lines are 60-point Savitzky-Golay filtered curves of the raw data.

larger at positive bias compared to negative bias, for both Ag bulk tips (see Fig. S12) as well as Ag-coated W tips. A strong polarity dependence of Ag-coated tips has also been observed previously,[29] but its origin is unclear as such behavior is not known for STM-LE of bare W tips.[26,30,31] However, an overall stronger intensity of the plasmon resonance at positive bias can directly explain the much larger switching rate shown in Fig. S11(b).

We conclude that within the HOMO-LUMO gap and below the threshold of the S_1 excited state, the shuttling motion can only be caused by direct plasmon-molecule coupling. Owing to the small threshold voltages at which shuttling starts to occur, we suggest that the most reasonable mechanism is vibrational excitation of the molecule from its S_0 ground state, which should be sufficient to overcome the energy barrier in the bistable orientation-dependent potential landscape.[18-20]

References

1 Kiraly, B. *et al.*, An orbitally derived single-atom magnetic memory, *Nat. Commun.* **9**, 3904 (2018).
2 Keizer, J. G., Garleff, J. K. & Koenraad, P. M., Simple and efficient scanning tunneling luminescence detection at low-temperature, *Rev. Sci. Instrum.* **80**, 123704 (2009).
3 Doppagne, B. *et al.*, Vibronic Spectroscopy with Submolecular Resolution from STM-Induced Electroluminescence, *Phys. Rev. Lett.* **118**, 127401 (2017).
4 Theisen, R. F., Huang, L., Fleetham, T., Adams, J. B. & Li, J., Ground and excited states of zinc phthalocyanine, zinc tetrabenzoporphyrin, and azaporphyrin analogs using DFT and TDDFT with Franck-Condon analysis, *J. Chem. Phys.* **142**, 094310 (2015).
5 Yanagisawa, S. *et al.*, Intermolecular Interaction as the Origin of Red Shifts in Absorption Spectra of Zinc-Phthalocyanine from First-Principles, *J. Phys. Chem. A* **117**, 11246 (2013).
6 Repp, J., Meyer, G., Stojkovic, S. M., Gourdon, A. & Joachim, C., Molecules on insulating films: Scanning-tunneling microscopy imaging of individual molecular orbitals, *Phys. Rev. Lett.* **94**, 026803 (2005).
7 Doležal, J. *et al.*, Mechano-Optical Switching of a Single Molecule with Doublet Emission, *ACS Nano* **14**, 8931 (2020).
8 Repp, J., Meyer, G., Paavilainen, S., Olsson, F. E. & Persson, M., Scanning Tunneling Spectroscopy of Cl Vacancies in NaCl Films: Strong Electron-Phonon Coupling in Double-Barrier Tunneling Junctions, *Phys. Rev. Lett.* **95**, 225503 (2005).
9 Doppagne, B. *et al.*, Single-molecule tautomerization tracking through space- and time-resolved fluorescence spectroscopy, *Nat. Nanotechnol.* **15**, 207 (2020).
10 Kröger, J., Doppagne, B., Scheurer, F. & Schull, G., Fano Description of Single-Hydrocarbon Fluorescence Excited by a Scanning Tunneling Microscope, *Nano Lett.* **18**, 3407 (2018).
11 Nian, L. L., Wang, Y. F. & Lu, J. T., On the Fano Line Shape of Single Induced by a Scanning Tunneling Molecule Electroluminescence Microscope, *Nano Lett.* **18**, 6826 (2018).
12 Fano, U., Effects of Configuration Interaction on Intensities and Phase Shifts, *Phys. Rev.* **124**, 1866 (1961).
13 Maksymovych, P., Dougherty, D. B., Zhu, X. Y. & Yates, J. T., Nonlocal dissociative chemistry of adsorbed molecules induced by localized electron injection into metal surfaces, *Phys. Rev. Lett.* **99**, 016101 (2007).
14 Leisegang, M., Kügel, J., Klein, L. & Bode, M., Analyzing the Wave Nature of Hot Electrons with a Molecular Nanoprobe, *Nano Lett.* **18**, 2165 (2018).
15 Ladenthin, J. N. *et al.*, Hot Carrier-Induced Tautomerization within a Single Porphycene Molecule on Cu(111), *ACS Nano* **9**, 7287 (2015).
16 Schendel, V. *et al.*, Remotely Controlled Isomer Selective Molecular Switching, *Nano Lett.* **16**, 93 (2016).
17 Kügel, J. *et al.*, Remote Single-Molecule Switching: Identification and Nanoengineering of Hot Electron-Induced Tautomerization, *Nano Lett.* **17**, 5106 (2017).
18 Stipe, B. C. *et al.*, Single-molecule dissociation by tunneling electrons, *Phys. Rev. Lett.* **78**, 4410 (1997).
19 Komeda, T., Kim, Y., Kawai, M., Persson, B. N. J. & Ueba, H., Lateral hopping of molecules induced by excitation of internal vibration mode, *Science* **295**, 2055 (2002).
20 Kumagai, T. *et al.*, Thermally and Vibrationally Induced Tautomerization of Single Porphycene Molecules on a Cu(110) Surface, *Phys. Rev. Lett.* **111**, 246101 (2013).
21 Braun, K. F., Soe, W. H., Flipse, C. F. J. & Rieder, K. H., Electromigration of single metal atoms observed by scanning tunneling microscopy, *Appl. Phys. Lett.* **90**, 023118 (2007).

22 Alemani, M. *et al.*, Electric field-induced isomerization of azobenzene by STM, *J. Am. Chem. Soc.* **128**, 14446 (2006).
23 Akimov, A. V. & Kolomeisky, A. B., Unidirectional Rolling Motion of Nanocars Induced by Electric Field, *J. Phys. Chem. C* **116**, 22595 (2012).
24 Patera, L. L., Queck, F., Scheuerer, P., Moll, N. & Repp, J., Accessing a Charged Intermediate State Involved in the Excitation of Single Molecules, *Phys. Rev. Lett.* **123**, 016001 (2019).
25 Peller, D. *et al.*, Sub-cycle atomic-scale forces coherently control a single-molecule switch, *Nature* **585**, 58 (2020).
26 Berndt, R., Gimzewski, J. K. & Johansson, P., Inelastic Tunneling Excitation of Tip-Induced Plasmon Modes on Noble-Metal Surfaces, *Phys. Rev. Lett.* **67**, 3796 (1991).
27 Johansson, P., Monreal, R. & Apell, P., Theory for light emission from a scanning tunneling microscope, *Phys. Rev. B* **42**, 9210 (1990).
28 Persson, B. N. J. & Baratoff, A., Theory of Photon-Emission in Electron-Tunneling to Metallic Particles, *Phys. Rev. Lett.* **68**, 3224 (1992).
29 Doležal, J. *et al.*, Charge Carrier Injection Electroluminescence with CO-Functionalized Tips on Single Molecular Emitters, *Nano Lett.* **19**, 8605 (2019).
30 Berndt, R. & Gimzewski, J. K., Isochromat spectroscopy of photons emitted from metal surfaces in an STM, *Ann. Phys.* **505**, 133 (1993).
31 Cavar, E. *et al.*, Fluorescence and phosphorescence from individual C_{60} molecules excited by local electron tunneling, *Phys. Rev. Lett.* **95**, 196102 (2005).